*electronics*

*Article*

# Steady-State Temperature-Sensitive Electrical Parameters' Characteristics of GaN HEMT Power Devices

**Kaihong Wang [1], Yidi Zhu [2], Hao Zhao [2], Ruixue Zhao [3] and Binxin Zhu [2,*]**

[1] Hubei Provincial Key Laboratory for Operation and Control of Cascaded Hydropower Station, China Three Gorges University, Yichang 443002, China; wangkaihong@ctgu.edu.cn
[2] Hubei Provincial Engineering Technology Research Center for Intelligent Energy Technology, China Three Gorges University, Yichang 443002, China; zhuyidi@ctgu.edu.cn (Y.Z.); zhaohao11@ctgu.edu.cn (H.Z.)
[3] College of Rail Transit, Hefei Technology College, Hefei 238010, China; zhaoruixue@htc.edu.cn
* Correspondence: zhubinxin40@163.com

**Abstract:** Gallium nitride high-electron-mobility transistor (GaN HEMT) power devices are favored in various scenarios due to their high-power density and efficiency. However, with the significant increase in the heat flux density, the junction temperature of GaN HEMT has become a crucial factor in device reliability. Since the junction temperature monitoring technology for GaN HEMT based on temperature-sensitive electrical parameters (TSEPs) is still in the exploratory stage, the TSEPs' characteristics of GaN HEMT have not been definitively established. In this paper, for the common steady-state TSEPs of GaN HEMT, the variation rules of the saturation voltage with low current injection, threshold voltage, and body-like diode voltage drop with temperature are investigated. The influences on the three TSEPs' characteristics are considered, and their stability is discussed. Through experimental comparison, it is found that the saturation voltage with low current injection retains favorable temperature-sensitive characteristics, which has potential application value in junction temperature measurement. However, the threshold voltage as a TSEP for certain GaN HEMT is not ideal in terms of linearity and stability.

**Keywords:** GaN HEMT; reliability; temperature-sensitive electrical parameters; junction temperature monitoring



**Citation:** Wang, K.; Zhu, Y.; Zhao, H.; Zhao, R.; Zhu, B. Steady-State Temperature-Sensitive Electrical Parameters' Characteristics of GaN HEMT Power Devices. *Electronics* **2024**, *13*, 363. https://doi.org/10.3390/electronics13020363

Academic Editor: Geok Ing Ng

Received: 24 November 2023
Revised: 3 January 2024
Accepted: 11 January 2024
Published: 15 January 2024



## 1. Introduction

As wide bandgap power semiconductor devices, Gallium nitride high-electron-mobility transistor (GaN HEMT) power devices have attractive advantages such as a fast switching speed, high switching frequency, and low conduction resistance, which penetrate fast chargers, data centers, 5G equipment, etc. [1–5]. With the decrease of GaN HEMTs' physical size and increase in the power density requirements, the heat flux density of the devices surges significantly. For example, the heat flux density of GaN HEMT is as high as 300 W/cm$^2$, about three times that of Si-based IGBTs, as shown in Figure 1 [6]. Since a high heat flux density causes the devices' junction temperature to increase, the junction temperature as a key reliability parameter for Si-based devices is also valuable for the reliability of GaN HEMT [7–9].

The junction temperature is important for the operating condition and reliability of the devices. Firstly, a high junction temperature deteriorates device performance by increasing conduction loss. Secondly, it serves as a major factor contributing to device failure, with the failure rate doubling for every 10 °C increase in the junction temperature [10,11]. The junction temperature is the primary parameter in the device lifetime model that is the basis for device health and lifetime assessment, prediction, and management [12,13]. Therefore, monitoring the junction temperature is a prerequisite for the efficient operation and reliable application of devices.

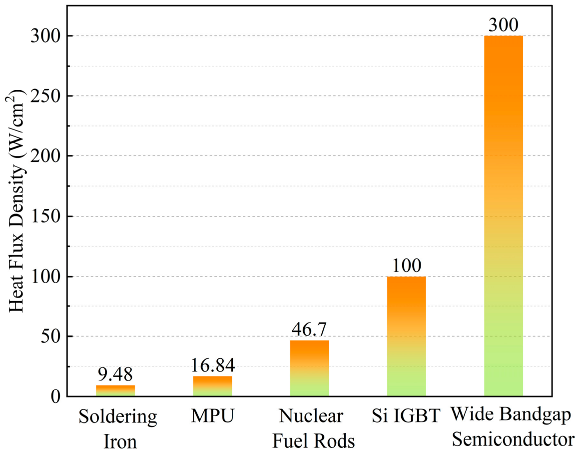


**Figure 1.** Heat flux density of different heat sources [6].

The junction temperature monitoring methods can be divided into four categories: the optical measurement method, physical contact method, thermal network modeling method, and temperature-sensitive electrical parameters (TSEPs) method. The optical method can provide a map of the temperature distribution, but it requires that the device must be unpacked [14,15]. Although the physical contact method is inexpensive and noninvasive, its slow response speed makes it difficult to track dynamic junction temperature accurately [16]. While the thermal network modeling method is noninvasive, it requires extensive calculations based on accurate and continuously updated thermal network models [17,18]. In contrast, the TSEPs method, which treats the device itself as a thermal sensor, is a promising junction temperature measurement method because of its low cost, noninvasiveness, and potential for real-time on-line monitoring [19,20]. The TSEPs method for GaN HEMT still faces challenges due to device packaging, noise, and aging [21].

According to the time-based characteristics of TSEPs, the junction temperature monitoring methods for GaN HEMT based on TSEPs can be divided into steady-state TSEPs and transient TSEPs. Steady-state TSEPs are the electrical parameters related to the junction temperature when the devices to be measured are in full conduction or full shutdown, such as the saturation voltage with low current injection [22]. Transient TSEPs are the electrical parameters related to the junction temperature of the devices to be tested during the transient switching process, such as turn-on delay time [23]. In comparison, the calibration method for steady-state TSEPs is simple and less susceptible to noise, but it faces the challenge of online application. Although transient TSEPs have the potential for real-time online extraction of the junction temperature, they are susceptible to interference during the measurement process.

Since the reliability research on GaN HEMT is still in the early stages, the TSEPs method and its related characteristics are still being explored [24]. Compared to the transient TSEPs of GaN HEMT [23,25], the steady-state TSEPs are the focus of current research. In [26], the threshold voltage exhibits a negative temperature coefficient, and a good linear relationship with junction temperature, whose sensitivity is about 0.84 mV/K. In [22], the saturation voltage with low current injection or conduction resistance can be utilized as TSEPs, exhibiting a positive temperature coefficient and good linearity, and is suitable for GaN HEMT with different gate structures. In [27], the body-like diode voltage has a positive temperature coefficient, but its sensitivity varies widely among different types of GaN HEMT. As mentioned in [28], the Schottky gate diode forward characteristics can be used effectively to measure the channel temperature of GaN HEMT, but this method is only applicable to GaN HEMT with Schottky gate structures. Similar to gate diode voltage, the gate current can only be used for GaN HEMT with Schottky gate structures and has a positive temperature coefficient and nonlinear characteristics [29]. In contrast, saturation voltage, threshold voltage, and body-like diode voltage devices are more universal as TESPs for GaN HEMT. However, the current research results solely address the relationship between TSEP and junction temperature under specific conditions. The characteristics of TSEP have not been explored, which cannot adequately provide comprehensive guidance for the junction temperature monitoring of GaN HEMT.

In this article, the temperature-sensitive characteristics of commonly used steady-state TSEPs in GaN HEMT are discussed, which is beneficial for the study of the junction temperature monitoring of the reliability of GaN HEMT. This paper is organized as follows. Section 1 emphasizes three measurement methods for TSEPs and the underlying physical mechanisms of temperature variation. Section 2 describes the construction of an experimental platform. Section 3 investigates the influence of different factors on the three types of TSEPs, with a focus on the stability of TSEPs. The results demonstrate that the saturation voltage with low current injection, as a steady-state TSEP, offers significant advantages for practical applications.

## 2. Measurement Method of Steady-State TESPs

### *2.1. Saturation Voltage with Low Current Injection*

Referring to the IGBT parameter measurement standard of IEC [30], the measurement circuit for saturation voltage with low current injection of GaN HEMT is shown in Figure 2. A voltage source ($V_{\mathrm{gss}}$) and a constant current source ($I_{\mathrm{m}}$) are used to provide the gate voltage and test current for the device under test (DUT).

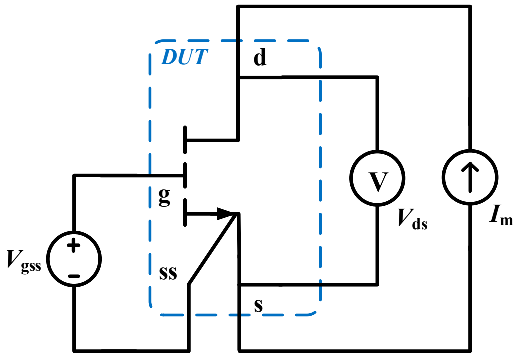


**Figure 2.** Measurement circuit for saturation voltage with low current injection.

When $V_{\mathrm{gss}} > V_{\mathrm{gss(th)}}$ and $V_{\mathrm{ds}} > 0$, GaN HEMT is in a forward conduction state. At this time, $V_{\mathrm{ds}}$ is defined as the drain-source voltage drop when forward conduction occurs, which can be expressed as [31]:

$$V_{\mathrm{ds}} = I_{\mathrm{ds}} \cdot \frac{L(d + \Delta d)}{W\mu\varepsilon(V_{\mathrm{gss}} - V_{\mathrm{gss(th)}})} \tag{1}$$

where $L$ is the channel length, $\Delta d$ is the channel thickness, $W$ is the gate width, and $d$ and $\varepsilon$ are the thickness and dielectric constant of the AlGaN barrier layer. $\mu$ is the electron mobility, $I_{\mathrm{ds}}$ is the drain current, $V_{\mathrm{gss}}$ is the gate voltage, and $V_{\mathrm{gss(th)}}$ is the gate threshold voltage.

Since the electron mobility $\mu$ decrease is sensitive to temperature $T$ and has negative temperature characteristics [32], $V_{\mathrm{ds}}$ increase with $\mu$ decrease when the drain of the device is injected into a constant test current. Thus, as a TSEP, the saturation voltage with low current injection has a positive temperature coefficient.

### *2.2. Threshold Voltage*

The threshold voltage is defined as the voltage applied to the device gate-source when the device drain is flowing the specified current at an ambient temperature. Typically, the specified drain current is in the $\mu$A or mA range [33]. Figure 3 shows the measurement circuit for the threshold voltage of the GaN HEMT. DUT is tested with the drain-gate shorted, and $I_m$ is the constant current source.

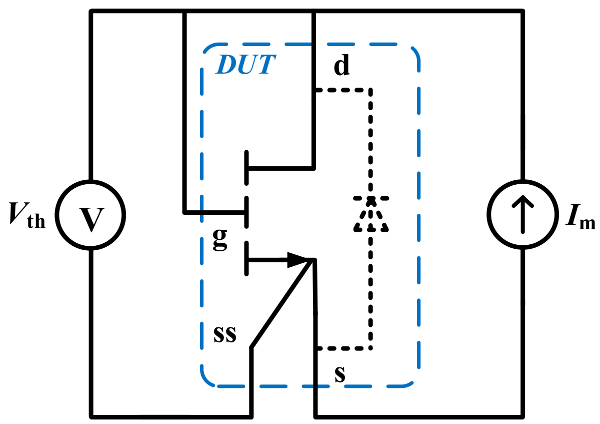


**Figure 3.** Measurement circuit for threshold voltage.

The threshold voltage of GaN HEMT can be expressed as [34]:

$$V_{th} = \phi_b - \Delta E_C - \frac{qN_d d^2}{2\varepsilon} - \frac{\sigma d}{\varepsilon} \tag{2}$$

where $\phi_b$ is the height of the potential barrier, $\Delta E_C$ is the conduction band discontinuity, $q$ is the charge and $N_d$ is the doping density, $\sigma$ is the total polarized charge density at the AlGaN/GaN interface, and $d$ and $\varepsilon$ are the thickness and dielectric constant of the AlGaN barrier layer.

Since the height of the potential barrier $\phi_b$, the conduction band discontinuity $\Delta E_C$, and the total polarized charge density at the AlGaN/GaN interface $\sigma$ exhibit significant positive temperature characteristics [35], the threshold voltage shows different trends as the temperature changes, depending on the dominant degree of $\phi_b$, $\Delta E_C$, and $\sigma$.

### *2.3. Body-like Diode Voltage*

Although there are no parasitic diodes in GaN HEMT, their reverse conduction characteristics are similar to MOSFETs [36]. Referring to the MOSFET body diode measurement method [37], the principle of the body-like diode voltage measurement for GaN HEMT is shown in Figure 4. $I_m$ provides the specified test current to the device, while $V_{gss}$ provides the specified gate voltage to turn off the device. Unlike the mechanism for measuring the saturation voltage with low current injection, the body-like diode voltage is typically measured by shorting or reverse biasing the gate and drain.

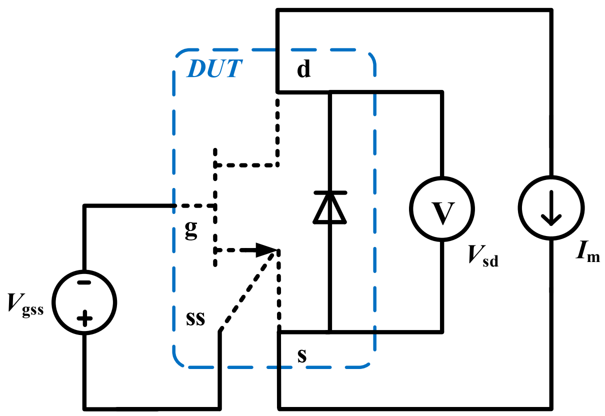


**Figure 4.** Measurement circuit for body-like diode voltage drop.

When $V_{gd} > V_{gd(th)}$, $V_{ds} < 0$, and $V_{gss} < V_{gss(th)}$, GaN HEMT is in a reverse conduction state. At this time, $V_{sd}$ is defined as the voltage drop between the source and drain during reverse conduction, which can be expressed as [36]:

$$V_{sd} = V_{gd(th)} - V_{gss} + I_{sd} \cdot R_{sd(on)} \tag{3}$$

where $V_{gd(th)}$ is the device reverse gate threshold voltage, $V_{gss}$ is the gate voltage, $I_{sd}$ is the drain source current, and $R_{sd(on)}$ is the reverse on resistance.

Since temperature affects both the reverse on resistance $R_{sd(on)}$ and the threshold voltage $V_{th}$, and the reverse on resistance $R_{sd(on)}$ has a positive temperature characteristic, the temperature characteristics of the body-like diode voltage $V_{sd}$ will correlate with those of the threshold voltage $V_{th}$ when a constant source drain current $I_{sd}$ is injected.

## 3. Experimental Investigation

### *3.1. Introduction of Experimental Platform*

Figure 5a depicts the experimental platform utilized to analyze the properties of three TSEPs, comprising saturation voltage with low current injection, threshold voltage, and body-like diode voltage. The DUT used for the test is the GaN HEMT model GS61008P produced by GaN Systems, the GaN HEMT model IGT60R070D1 produced by Infineon, and the SiC MOSFET model CMF20120D produced by Cree. To mitigate the impact of the temperature on the testing circuit, a split structure is employed. The PCB substrate containing only DUT is placed on the temperature control platform for separate heating, while other test circuits are connected to the substrate via the interface. The drive circuit is utilized to regulate the on–off state of the DUT. The constant current circuit provides a steady test current. To capture feeble variations in signals, the conditioning circuit houses an instrument amplifier that boasts high gain and an outstanding common mode rejection ratio.

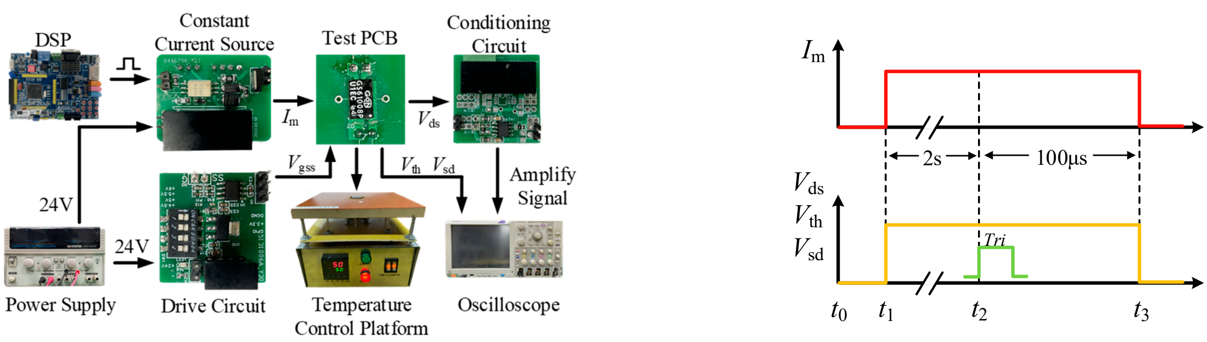


(**a**) (**b**)

**Figure 5.** Introduction of experimental platform: (**a**) platform layout; (**b**) measurement timing diagram.

During the test, the temperature control platform is set to 25 °C, 50 °C, 75 °C, 100 °C, and 125 °C, respectively. Each temperature point is maintained for 10 min to ensure that the DUT reaches the thermal equilibrium, which can be interpreted as the device junction temperature being equal to the temperature point. Considering that the components in the test circuit would be affected by temperature, the maximum temperature is set to 125 °C to evaluate the characteristics of TSEP. Figure 5b shows the measurement timing diagram. The pulsed $I_m$ is injected into the DUT. After 2 s, the data acquisition is triggered to ensure that the platform is in a stable state. The data are collected during 100 μs after the trigger signal, with the experimental error reduced by multiple measurements and average processing.

### *3.2. Drive Circuit*

To evaluate the effect of the drive voltage on the TSEP characteristics, the adjustable drive circuit is designed as shown in Figure 6, including the conventional drive circuit with

SI8271GB-IS and the adjustable voltage unit with LM317 to achieve stable and low-noise output voltage. The adjustable voltage $V_{cc}$ provided to the drive chip is adjusted through resistor $R_1$ and $R_2$, and is fed to the device gate.

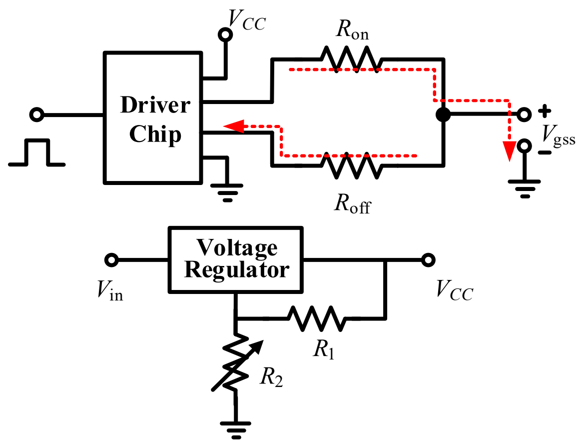


**Figure 6.** Adjustable drive circuit.

### *3.3. Constant Current Circuit*

A controllable constant current source circuit capable of providing a pulse type test current in milliampere levels is illustrated in Figure 7. Transistor $Q_1$ operates in an amplified state where the base current can be disregarded, and the output collector current $I_c$ is about equal to the emitter current $I_e$, that is:

$$I_c \approx I_e = \frac{U_{ZD1} - U_{eb}}{R_1} \tag{4}$$

where $U_{ZD1}$ is the voltage drop across the Zener diode $ZD_1$, and $U_{eb}$ is the voltage between the emitter and base, about 0.7 V. The constant current source output can be adjusted by resistance $R_1$. In addition, $R_2$ is used to limit the current and provide a steady-state operating point for $ZD_1$. The optocoupler chip ACPL-P346 with electrical isolation is used to control the voltage $V_{out}$ fed to a constant current circuit.

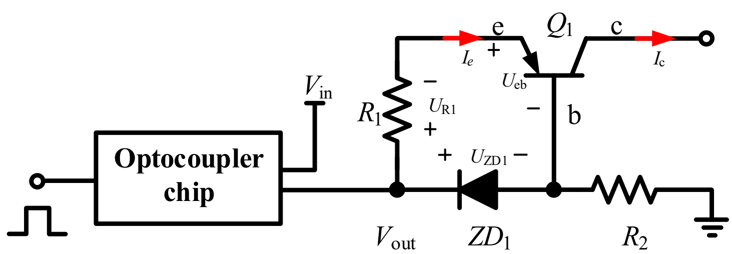


**Figure 7.** Constant current circuit.

### *3.4. Conditioning Circuit*

In order to accurately measure the weak voltage signal, the conditioning circuit constructed with the instrument amplifier AD8221 is shown in Figure 8, where the resistance $R_1$ is 49.4 kΩ. The external resistance $R_G$ is used to adjust the voltage gain. The resistance $R$ and the capacitor $C_C$ form two groups of low-pass $RC$ networks to filter the high-frequency signals and suppress common mode interference, while the capacitor $C_D$ affects the differential signal. The gain $G$ of the conditioning circuit is:

$$G = 1 + \frac{R_1}{R_G} = 1 + \frac{49.4\text{k}\Omega}{R_G} \tag{5}$$

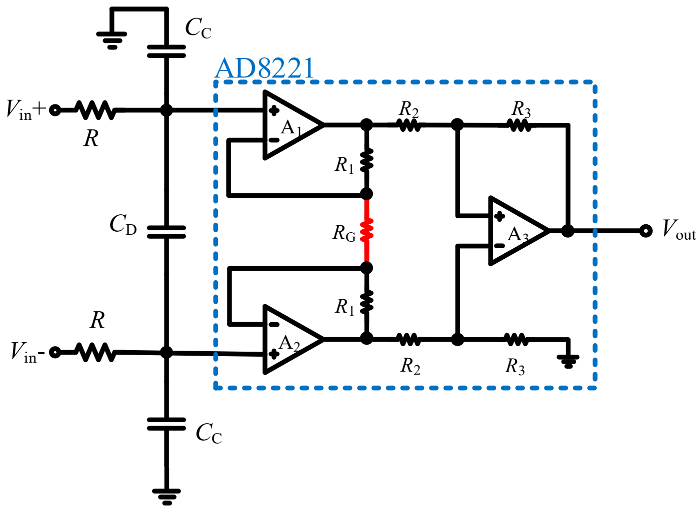


**Figure 8.** Conditioning circuit.

To fulfill the measurement requirements, the gain is set to 495 in this paper, and the external resistance $R_G$ is 100 Ω. For a nonperiodic rectangular pulse signal with a pulse amplitude of $A$ and a pulse width of $\tau$, the spectrum is [38]:

$$X(\mathrm{j}\omega) = \frac{2A}{\omega}\sin\left(\frac{\omega\tau}{2}\right) \tag{6}$$

The instrument amplifier used in this paper has a corner frequency of about 5.5 kHz at a given 495 times gain, and an angular frequency $\omega_1$ of about 11,000$\pi$ rad/s. According to (6), the signal spectrum at $\omega_1$ is close to 0. Therefore, the high frequency signal with angular frequencies outside $\omega_1$ can be ignored, and the input voltage signal can be completely collected by the instrument amplifier.

## 4. Experimental Results and Analysis

### *4.1. Characteristics of Saturation Voltage with Low Current Injection*

Based on the measurement circuit shown in Figure 2 and information from the DUT datasheet, the gate voltage $V_{gss}$ is set to 5 V and the test current $I_m$ is set to 300 mA. The $V_{ds}$-$T_j$ curves of two GaN HEMT device models GS61008P are shown in Figure 9. It can be seen that a saturation voltage with low current injection $V_{ds}$ increases with the junction temperature $T_j$, which is consistent with the theoretical analysis. In addition, the $V_{ds}$ has good linearity, whose fitting coefficient reaches approximately 0.998. However, $V_{ds}$ has a temperature sensitivity of about 0.015 mV/°C and is much smaller than that of Si-based (2 mV/°C) and SiC-based devices (5 mV/°C) [10,39], which is a challenge for utilizing $V_{ds}$ as a TSEP to extract the junction temperature of GaN HEMT.

To explore the influence of $I_m$ on the temperature sensitivity of $V_{ds}$, $V_{gss}$ is kept at 5 V, and $I_m$ is successively increased from 100 mA to 300 mA. $V_{ds}$-$T_j$ curves under different $I_m$ are shown in Figure 10a. It can be seen that the saturation voltage with low current injection of GaN is the function of the test current and the junction temperature. Similar to IGBT devices, $V_{ds}$ demonstrates nonlinear variation with $I_m$ at a given temperature [40]. The sensitivity of this TSEP depends on the test current $I_m$ level. As the $I_m$ decreases, the sensitivity of $V_{ds}$ declines from 0.016 mV/°C to 0.006 mV/°C, which makes the measurement of $V_{ds}$ more difficult. Conversely, increasing $I_m$ improves the sensitivity of $V_{ds}$, but it can lead to self-heating during junction temperature monitoring. According to the thermal resistance from the junction to case $R_{\Theta JC}$ and the power dissipation $P$, the temperature difference from the junction to case under steady-state is

$$\Delta T = P \times R_{\Theta JC} \tag{7}$$

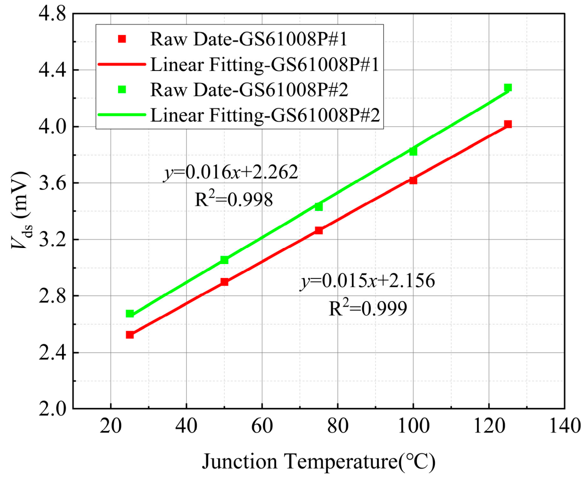


**Figure 9.** Temperature characteristics of $V_{ds}$.

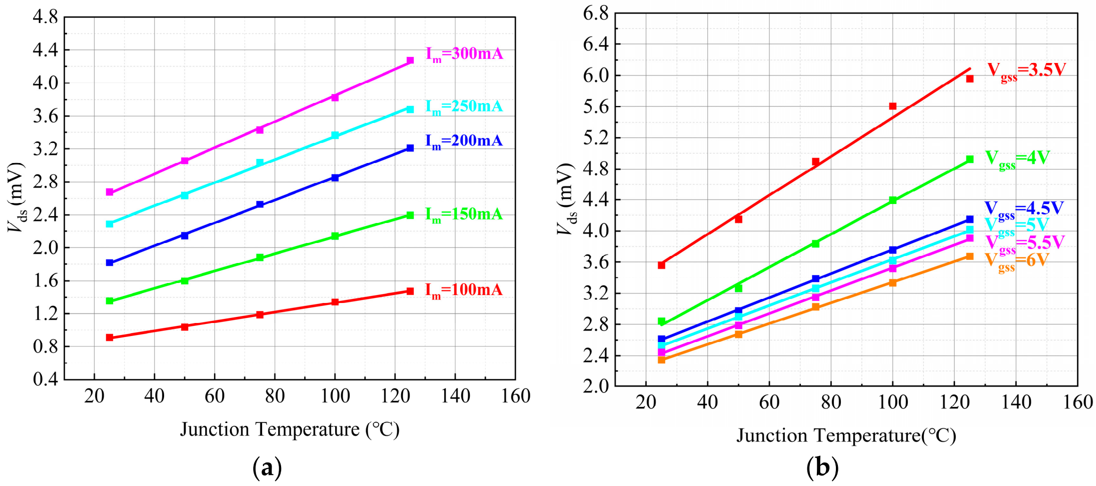


**Figure 10.** Relationship between $V_{ds}$ and junction temperature under different test conditions: (**a**). under different $I_m$; (**b**). under different $V_{gss}$.

Since $R_{\Theta JC}$ is 0.55 °C/W based on the datasheet and the maximum $I_m$ is 300 mA, the temperature difference from the junction to case is far less than 0.001 °C, which can be ignored.

To explore the effect of $V_{gss}$ on the temperature sensitivity of $V_{ds}$, $I_m$ is set to 300 mA, and $V_{gss}$ ranges from 3.5 V to 6 V. $V_{ds}$-$T_j$ curves under different $V_{gss}$ are shown in Figure 10b. It can be seen that the larger $V_{gss}$ is, the better the linear fitting is. However, the sensitivity of $V_{ds}$ reduces from 0.025 mV/°C to 0.013 mV/°C. Specifically, when $V_{gss}$ is between about 4.5 V and 6 V, the sensitivity changes slightly within the range of 0.013 mV/°C to 0.015 mV/°C, from which it can be inferred that the conductive channel resistance characteristics are affected by $V_{gss}$. When $V_{gss}$ is low, the conductive channel resistance and its sensitivity change significantly with $V_{gss}$, and the temperature sensitivity of $V_{ds}$ is easily affected by $V_{gss}$. Conversely, when the sensitivity of conductive channel resistance tends to be stable with the increase of $V_{gss}$, the influence of $V_{gss}$ on the temperature sensitivity of $V_{ds}$ is weak.

### 4.2. Characteristics of Threshold Voltage

The test current $I_m$ of 10 mA is used, based on the schematic diagram presented in Figure 3 and information from the DUT datasheet. Figure 11 shows the $V_{th}$-$T_j$ curves of two GaN HEMT devices of model GS61008P. Unlike that of Si-based devices and SiC-based MOSFET devices [41,42], the threshold voltage $V_{th}$ of the GaN HEMT has a positive temperature coefficient, probably because the temperature-dependent behavior of the barrier height plays a dominant role based on (2). Additionally, the sensitivity range of $V_{th}$ is between 1.6 mV/°C and 1.9 mV/°C, which is smaller than that of the Si-based device [43]. The fitting coefficient of $V_{th}$ is weaker than that of $V_{ds}$.

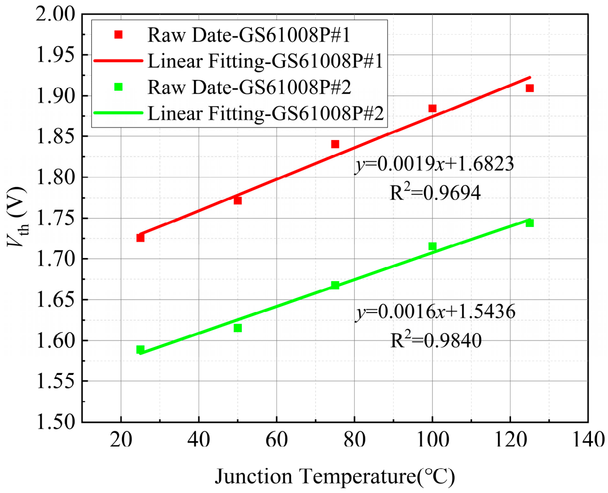


**Figure 11.** Temperature characteristics of $V_{th}$.

To explore the influence of $I_m$ on the temperature-sensitive characteristics of $V_{th}$, $I_m$ is set to 5 mA, 10 mA, 15 mA, and 20 mA, respectively. The $V_{th}$-$T_j$ curves under different $I_m$ are shown in Figure 12. It can be seen that $V_{th}$ rises with $I_m$ and exhibits a level of discreteness in contrast to $V_{ds}$.

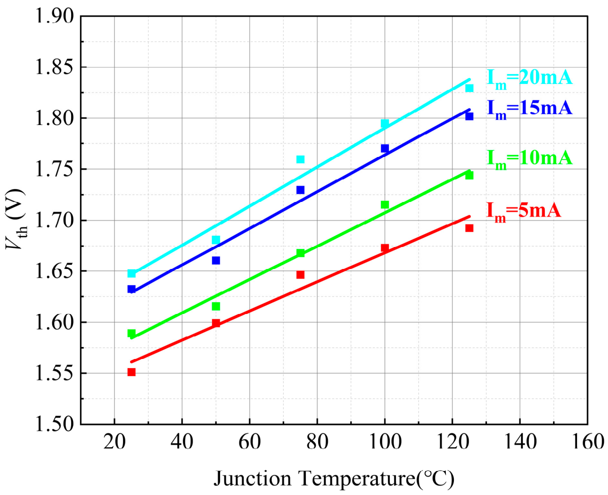


**Figure 12.** Relationship between $V_{th}$ and junction temperature under different $I_m$.

*4.3. Characteristics of Body-like Diode Voltage*

Based on the measurement circuit shown in Figure 4, the constant current $I_m$ is set to 100 mA, and the gate voltage $V_{gss}$ is set to 0 V. The $V_{sd}$-$T_j$ curves of the two GaN HEMT devices of model GS61008P are presented in Figure 13. It can be seen that $V_{sd}$ of the body-like diode increases with the junction temperature. Based on (3), the threshold voltage and resistance, which have positive temperature characteristics, make $V_{sd}$ also have positive temperature characteristics. Additionally, $V_{sd}$ exhibits excellent linearity, whose fitting coefficient reaches approximately 0.98. The DUT's $V_{sd}$ has a temperature sensitivity of about 2 mV/°C, which is comparable to the body diode voltage drop sensitivity of 2.4 mV/°C for SiC MOSFET [37].

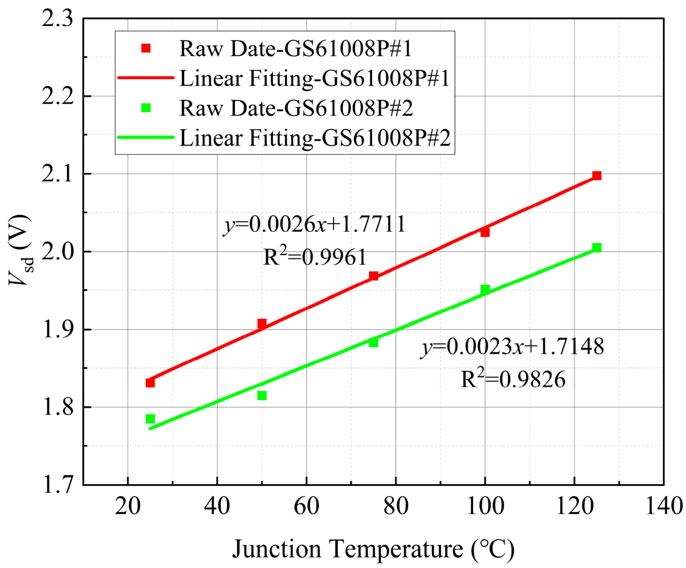


**Figure 13.** Temperature characteristics of $V_{sd}$.

To explore the effect of $I_m$ on the temperature sensitivity of the $V_{sd}$, $V_{gss}$ is kept at 0 V, and $I_m$ is set to several groups of values. The relationship between $V_{sd}$ and junction temperature under different $I_m$ is shown in Figure 14. It is evident that the $V_{sd}$ maintains good linearity, and the initial value of $V_{sd}$ has a slight increase while the sensitivity remains relatively constant as $I_m$ increases. Within the set range of $I_m$, $V_{sd}$ has a temperature sensitivity that remains around 2 mV/°C.

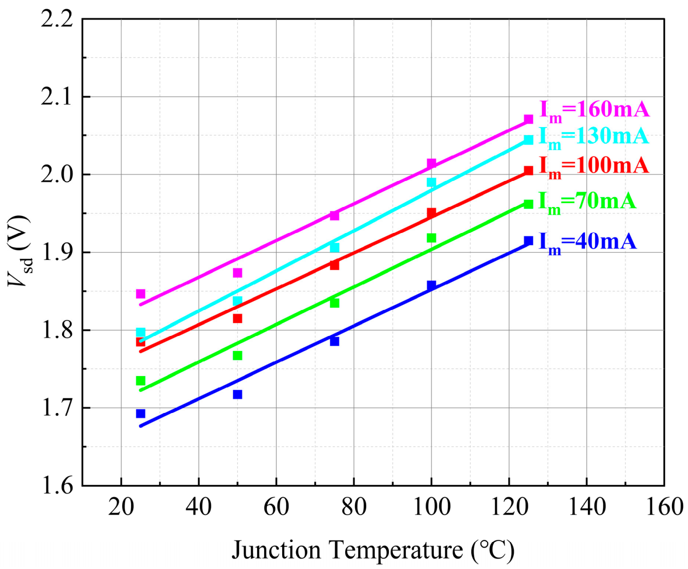


**Figure 14.** Relationship between $V_{sd}$ and junction temperature under $I_m$.

### *4.4. Stability of TSEPs' Characteristics under Temperature Cycles*

After subjecting the DUT to temperature cycling in the experiment, the TSEPs show parameter drift under identical test conditions, thus indicating inconsistent stability. The temperature cycle specifically refers to the use of natural cooling to cool down DUT after the test temperature reaches the maximum temperature, and then DUT is tested for the next cycle. To improve the precision of results during temperature cycles, multiple measurements are performed at each temperature point.

To explore the stability of TSEPs, Infineon's product GaN HEMT IGT60R070D1 and Cree's product SiC MOSFET CMF20120D are used in the experiment and compared with GaN System's product GaN HEMT GS61008P used in the previous section.

The stability of three parameters is tested: saturation voltage with low current injection $V_{ds}$, threshold voltage $V_{th}$, and body-like diode voltage $V_{sd}$. For the stability of $V_{ds}$, each DUT is subjected to three temperature cycles and the test current of 300 mA is injected. Due to different material characteristics and voltage levels, the initial $V_{ds}$ value of each device is also different. Table 1 displays the $V_{ds}$, $V_{th}$, and $V_{sd}$ of each device measured at 25 °C. $V_{ds}$ of GS61008P is significantly smaller than that of IGT60R070D1 and CMF20120D. To better illustrate the TSEPs' characteristics, the results are normalized as shown in Figure 15. The curve overlap of all devices is good during three temperature cycles, which indicates that $V_{ds}$ has good stability and the impact of the temperature cycles on $V_{ds}$ can be negligible. It is beneficial to the application of $V_{ds}$ in junction temperature measurement. Furthermore, according to the experimental results, the sensitivity of the GaN HEMT device is significantly lower than that of SiC MOSFET. Therefore, utilizing $V_{ds}$ as a TSEP is more challenging in the junction temperature extraction of GaN HEMT [22,39].

**Table 1.** Initial TSEPs' values measured at 25 °C.

| | GaN HEMT GS61008P | GaN HEMT IGT60R070D1 | SiC MOSFET CMF20120D |
|---|---|---|---|
| $V_{ds}$ (mV) | 2.57 | 16.72 | 297 |
| $V_{th}$ (V) | 2.09 | 1.47 | 5.22 |
| $V_{sd}$ (mV) | 1.83 | 1.51 | 0.56 |

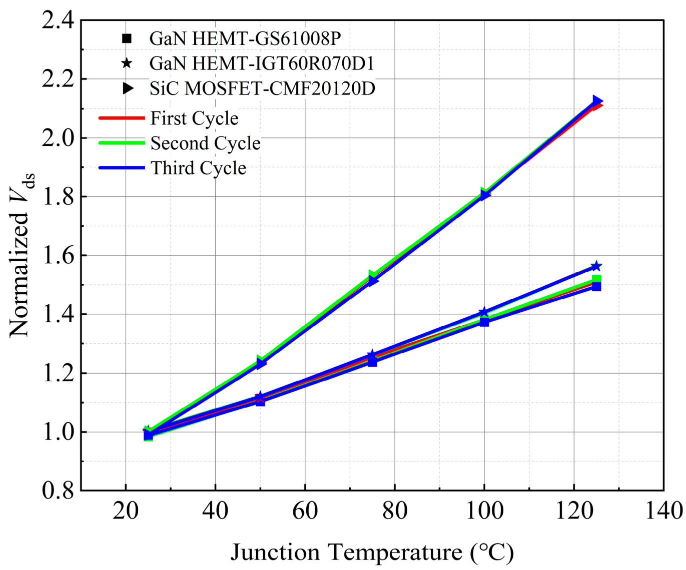


**Figure 15.** Normalized $V_{ds}$ of different devices under temperature cycle.

For the stability of the threshold voltage $V_{th}$, each device is subjected to three temperature cycles, and the test current of 10 mA is applied. The $V_{th}$ of the three devices measured at the initial temperature of 25 °C is shown in Table 1. The normalized $V_{th}$ of each device is shown in Figure 16. It can be seen that the $V_{th}$ of GS61008P fluctuates significantly, while IGT60R070D1 and CMF20120D have better stability, which indicates that the stability of $V_{th}$ needs to be considered when it is used as the TSEP of GaN HEMT. Additionally, the linearity of GS61008P is notably weaker compared to that of IGT60R070D1 and CMF20120D. In particular, for GaN HEMTs GS61008P and IGT60R070D1, the $V_{th}$ of the two devices presents opposite temperature characteristics, which may be caused by the dominant degree of $\phi_b$, $\Delta E_C$, and $\sigma$ of the two devices at different temperatures.

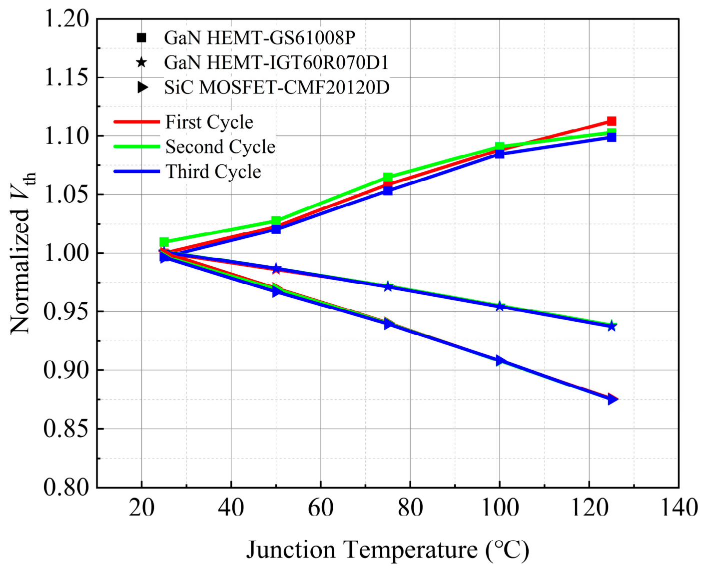


**Figure 16.** Normalized $V_{th}$ of different devices under temperature cycle.

For the stability of the body-like diode $V_{sd}$, each device is subjected to three temperature cycles with the gate voltage set to 0 V and a test current of 100 mA. GaN HEMT exhibits a higher $V_{sd}$ than SiC MOSFET at 25 °C, per Table 1. The normalized $V_{sd}$ of each device is presented in Figure 17. It is evident that the $V_{sd}$ of IGT60R070D1 and CMF20120D exhibits stability, whereas the $V_{sd}$ of GS61008P has slight fluctuations, which are much smaller than those of the $V_{th}$ in the same device. In addition, compared to the positive temperature characteristics of GS61008P, the $V_{sd}$ of IGT60R070D1 as a GaN HEMT exhibits negative temperature characteristics, which are caused by the negative temperature characteristics of $V_{th}$ based on Equation (3).

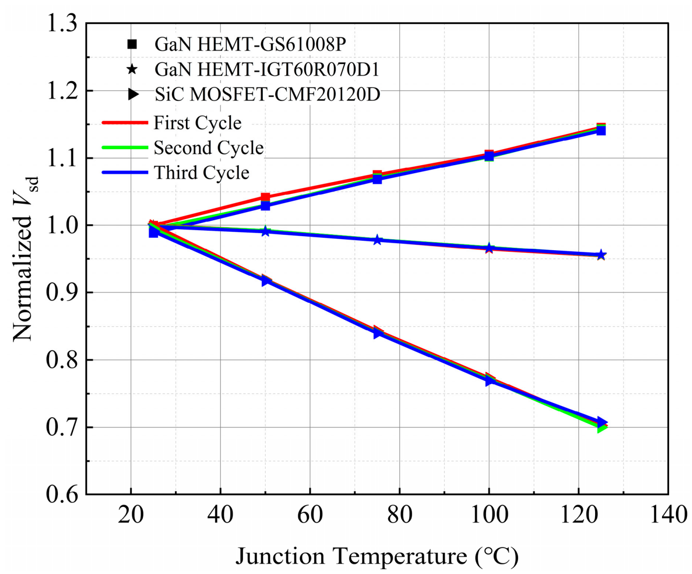


**Figure 17.** Normalized $V_{sd}$ of different devices under temperature cycle.

## 5. Conclusions

Currently, the junction temperature monitoring of GaN HEMT based on the TSEPs method remains in the exploratory stage. Research on the characteristics of steady-state TSEPs is beneficial to their application in device reliability. This article presents test guidelines for three TSEPs, saturation voltage with low current injection, threshold voltage, and body-like diode voltage, and focuses on investigating their stability and assessing their temperature-sensitive characteristics. The following conclusions can be drawn:

1. The saturation voltage with low current injection as a TSEP still has good temperature-sensitive characteristics, showing good linearity and stability in GaN HEMT. Its sensitivity is influenced by both the injection current and gate voltage. Overall, it has potential value in the field of temperature measurement.
2. The threshold and body-like diode voltage as TSEPs exhibit significant variations for different devices. In particular, for some GaN HEMT, the stability of the threshold voltage is not ideal, which needs to be considered in applications.
3. Compared to Si and SiC devices, the sensitivity of TSEPs in GaN HEMT is generally lower, especially saturation voltage with low current injection, which poses higher challenges to their application in junction temperature monitoring.

**Author Contributions:** Writing—Original Draft: K.W. and Y.Z.; Writing—Reviewing and Editing: K.W., Y.Z. and H.Z.; Supervision: R.Z. and B.Z. All authors have read and agreed to the published version of the manuscript.

**Funding:** This work was funded by Yichang Natural Science Research Project (A23-2-019) and Hubei Provincial Key Laboratory for Operation and Control of Cascaded Hydropower Station (2021KJX07 and 2022KJX08).

**Data Availability Statement:** Data are contained within the article.

**Conflicts of Interest:** The authors declare no conflicts of interest.

## References

1. Gonzalez, J.O.; Wu, R.; Jahdi, S.; Alatise, O. Performance and Reliability Review of 650 V and 900 V Silicon and SiC Devices: MOSFETs, Cascode JFETs and IGBTs. *IEEE Trans. Ind. Electron.* **2020**, *67*, 7375–7385. [CrossRef]
2. Zhu, B.; Liu, J.; Liu, Y.; Wang, K. Fault-Tolerance Wide Voltage Conversion Gain DC/DC Converter for More Electric Aircraft. *Chin. J. Aeronaut.* **2023**, *36*, 420–429. [CrossRef]
3. Gareau, J.; Hou, R.; Emadi, A. Review of Loss Distribution, Analysis, and Measurement Techniques for GaN HEMTs. *IEEE Trans. Power Electron.* **2020**, *35*, 7405–7418. [CrossRef]
4. Zhu, B.; Yang, Y.; Wang, K.; Liu, J.; Vilathgamuwa, D.M. High Transformer Utilization Ratio and High Voltage Conversion Gain Flyback Converter for Photovoltaic Application. *IEEE Trans. Ind. Appl.* **2023**, 1–13. [CrossRef]
5. Zhu, B.; Zeng, Q.; Chen, Y.; Zhao, Y.; Liu, S. A Dual-Input High Step-Up DC/DC Converter With ZVT Auxiliary Circuit. *IEEE Trans. Energy Convers.* **2019**, *34*, 161–169. [CrossRef]
6. Suganuma, K. *Power Semiconductor Devices*; The Nikkan Kogyo Shimbun: Tokyo, Japan, 2014; ISBN 978-4-526-07339-7.
7. Yang, Y.; Zhang, P. In Situ Insulated Gate Bipolar Transistor Junction Temperature Estimation Method via a Bond Wire Degradation Independent Parameter Turn-OFF $V_{ce}$ Overshoot. *IEEE Trans. Ind. Electron.* **2021**, *68*, 10118–10129. [CrossRef]
8. Mandeya, R.; Chen, C.; Pickert, V.; Naayagi, R.T. Prethreshold Voltage as a Low-Component Count Temperature Sensitive Electrical Parameter Without Self-Heating. *IEEE Trans. Power Electron.* **2018**, *33*, 2787–2791. [CrossRef]
9. Wang, K.; Zhou, L.; Sun, P.; Du, X. Monitoring Bond Wire Defects of IGBT Module Using Module Transconductance. *IEEE J. Emerg. Sel. Top. Power Electron.* **2021**, *9*, 2201–2211. [CrossRef]
10. Deng, E.; Borucki, L.; Lutz, J. Correction of Delay-Time-Induced Maximum Junction Temperature Offset During Electrothermal Characterization of IGBT Devices. *IEEE Trans. Power Electron.* **2021**, *36*, 2564–2573. [CrossRef]
11. Hu, Z.; Zhang, W.; Wu, J. An Improved Electro-Thermal Model to Estimate the Junction Temperature of IGBT Module. *Electronics* **2019**, *8*, 1066. [CrossRef]
12. Baker, N.; Liserre, M.; Dupont, L.; Avenas, Y. Improved Reliability of Power Modules: A Review of Online Junction Temperature Measurement Methods. *IEEE Ind. Electron. Mag.* **2014**, *8*, 17–27. [CrossRef]
13. Wang, K.; Zhou, L.; Sun, P.; Du, X. Monitoring Bond Wires Fatigue of Multichip IGBT Module Using Time Duration of the Gate Charge. *IEEE Trans. Power Electron.* **2021**, *36*, 888–897. [CrossRef]
14. Bagnall, K.R.; Moore, E.A.; Badescu, S.C.; Zhang, L.; Wang, E.N. Simultaneous Measurement of Temperature, Stress, and Electric Field in GaN HEMTs with Micro-Raman Spectroscopy. *Rev. Sci. Instrum.* **2017**, *88*, 113111. [CrossRef] [PubMed]
15. Isa, R.; Mirza, J.; Ghafoor, S.; Mustafa Khan, M.Z.; Qureshi, K.K. Junction Temperature Optical Sensing Techniques for Power Switching Semiconductors: A Review. *Micromachines* **2023**, *14*, 1636. [CrossRef] [PubMed]
16. Hu, Z.; Du, M.; Wei, K.; Hurley, W.G. An Adaptive Thermal Equivalent Circuit Model for Estimating the Junction Temperature of IGBTs. *IEEE J. Emerg. Sel. Top. Power Electron.* **2019**, *7*, 392–403. [CrossRef]
17. Zhou, Z.; Sui, Y.; Zhang, X.; Tong, C.; Zheng, P.; Zhu, M. IGBT Temperature Field Monitoring Based on Reduced-Order Model. *CES Trans. Electr. Mach. Syst.* **2023**, *7*, 129–136. [CrossRef]

18. An, T.; Zhou, R.; Qin, F.; Dai, Y.; Gong, Y.; Chen, P. Comparative Study of the Parameter Acquisition Methods for the Cauer Thermal Network Model of an IGBT Module. *Electronics* **2023**, *12*, 1650. [CrossRef]
19. Lu, S.; Zhang, Z.; Buttay, C.; Ngo, K.D.T.; Lu, G.-Q. Improved Measurement Accuracy for Junction-to-Case Thermal Resistance of GaN HEMT Packages by Gate-to-Gate Electrical Resistance and Stacking Thermal Interface Materials. *IEEE Trans. Power Electron.* **2022**, *37*, 6285–6289. [CrossRef]
20. Yang, F.; Pu, S.; Xu, C.; Akin, B. Turn-on Delay Based Real-Time Junction Temperature Measurement for SiC MOSFETs With Aging Compensation. *IEEE Trans. Power Electron.* **2021**, *36*, 1280–1294. [CrossRef]
21. Li, X.; Feng, S.; Liu, C.; Zhang, Y.; Bai, K.; Xiao, Y.; Zheng, X.; He, X.; Pan, S.; Lin, G.; et al. A Drain–Source Connection Technique: Thermal Resistance Measurement Method for GaN HEMTs Using TSEP at High Voltage. *IEEE Trans. Electron Devices* **2020**, *67*, 5454–5459. [CrossRef]
22. Shan, Y.; Gao, W.; Huang, Z.; Kuang, W.; Wu, Z.; Zhang, B. Test Methods and Principles of Thermal Resistance for GaN HEMT Power Devices. In Proceedings of the 2020 21st International Conference on Electronic Packaging Technology, Guangzhou, China, 12–15 August 2020; pp. 1–4.
23. Pan, S.; Feng, S.; Zheng, X.; He, X.; Li, X.; Bai, K. Effects of Temperature and Bias Voltage on Electron Transport Properties in GaN High-Electron-Mobility Transistors. *IEEE Trans. Device Mater. Reliab.* **2021**, *21*, 494–499. [CrossRef]
24. McDonald, T.; Butler, S.W. Progress and Current Topics of JEDEC JC-70.1 Power GaN Device Quality and Reliability Standards Activity: Or: What Is the Avalanche Capability of Your GaN Transistor? In Proceedings of the 2021 IEEE International Reliability Physics Symposium (IRPS), Monterey, CA, USA, 21–25 March 2021; pp. 1–6.
25. Hedayati, M.H.; Wang, J.; Dymond, H.C.P.; Liu, D.; Stark, B.H. Overtemperature Protection Circuit for GaN Devices Using a Di/Dt Sensor. *IEEE Trans. Power Electron.* **2021**, *36*, 7417–7428. [CrossRef]
26. Sharma, K.; Muñoz Barón1, K.; Ruthardt, J.; Kallfass, I. Characterisation of the Junction Temperature of Gallium-Nitride Power Devices via Quasi-Threshold Voltage as Temperature Sensitive Electrical Parameter. In Proceedings of the 10th International Conference on Power Electronics, Machines and Drives (PEMD 2020), Online, 15–17 December 2020; Volume 2020, pp. 932–936.
27. Franke, J.; Zeng, G.; Winkler, T.; Lutz, J. Power Cycling Reliability Results of GaN HEMT Devices. In Proceedings of the 2018 IEEE 30th International Symposium on Power Semiconductor Devices and ICs (ISPSD), Chicago, IL, USA, 13–17 May 2018; pp. 467–470.
28. Zheng, X.; Feng, S.; Zhang, Y.; Li, J. Evaluation of the Schottky Contact Degradation on the Temperature Transient Measurements in GaN HEMTs. *IEEE Trans. Electron Devices* **2018**, *65*, 1734–1738. [CrossRef]
29. Borghese, A.; Riccio, M.; Longobardi, G.; Maresca, L.; Breglio, G.; Irace, A. Gate Leakage Current Sensing for in Situ Temperature Monitoring of P-GaN Gate HEMTs. *Microelectron. Reliab.* **2020**, *114*, 113762. [CrossRef]
30. *IEC60747-9*; Semiconductor Devices Discrete Devices Part 9: Insluated-Gate Biploar Transistors (IGBTs). International Electrotechnical Commission: Geneva, Switzerland, 2007; pp. 60747–60749.
31. Rashmi; Kranti, A.; Haldar, S.; Gupta, R.S. An Accurate Charge Control Model for Spontaneous and Piezoelectric Polarization Dependent Two-Dimensional Electron Gas Sheet Charge Density of Lattice-Mismatched AlGaN/GaN HEMTs. *Solid-State Electron.* **2002**, *46*, 621–630. [CrossRef]
32. Chattopadhyay, M.K.; Tokekar, S. Thermal Model for Dc Characteristics of Algan/Gan Hemts Including Self-Heating Effect and Non-Linear Polarization. *Microelectron. J.* **2008**, *39*, 1181–1188. [CrossRef]
33. Huang, A. Infineon OptiMOSTMPower MOSFET Datasheet Explanation. 2012. Available online: https://www.infineon.com/dgdl/Infineon-MOSFET_OptiMOS_datasheet_explanation-AN-v01_00-EN.pdf?fileId=db3a30433b47825b013b6b8c6a3424c4 (accessed on 16 March 2022).
34. Rashmi; Kranti, A.; Haldar, S.; Gupta, M.; Gupta, R.S. Comprehensive Analysis of Small-Signal Parameters of Fully Strained and Partially Relaxed High Al-Content Lattice Mismatched Al/Sub m/Ga/Sub 1-m/N/GaN HEMTs. *IEEE Trans. Microw. Theory Tech.* **2003**, *51*, 607–617. [CrossRef]
35. Alim, M.A.; Rezazadeh, A.A.; Gaquiere, C. Temperature Dependence of the Threshold Voltage of AlGaN/GaN/SiC High Electron Mobility Transistors. *Semicond. Sci. Technol.* **2016**, *31*, 125016. [CrossRef]
36. Jones, E.A.; Wang, F.; Ozpineci, B. Application-Based Review of GaN HFETs. In Proceedings of the 2014 IEEE Workshop on Wide Bandgap Power Devices and Applications, Knoxville, TN, USA, 13–15 October 2014; pp. 24–29.
37. González, J.A.O.; Alatise, O. A Novel Non-Intrusive Technique for BTI Characterization in SiC Mosfets. *IEEE Trans. Power Electron.* **2019**, *34*, 5737–5747. [CrossRef]
38. Chen, H. *Signals and Systems*; Prentice Hall: Upper Saddle River, NJ, USA, 2007; ISBN 978-7-04-022523-5.
39. Griffo, A.; Wang, J.; Colombage, K.; Kamel, T. Real-Time Measurement of Temperature Sensitive Electrical Parameters in SiC Power MOSFETs. *IEEE Trans. Ind. Electron.* **2018**, *65*, 2663–2671. [CrossRef]
40. Avenas, Y.; Dupont, L.; Khatir, Z. Temperature Measurement of Power Semiconductor Devices by Thermo-Sensitive Electrical Parameters—A Review. *IEEE Trans. Power Electron.* **2012**, *27*, 3081–3092. [CrossRef]
41. Zeng, G.; Cao, H.; Chen, W.; Lutz, J. Difference in Device Temperature Determination Using P-n-Junction Forward Voltage and Gate Threshold Voltage. *IEEE Trans. Power Electron.* **2019**, *34*, 2781–2793. [CrossRef]

42. Jiang, X.; Wang, J.; Yu, H.; Chen, J.; Zeng, Z.; Yang, X.; Shen, Z.J. Online Junction Temperature Measurement for SiC MOSFET Based on Dynamic Threshold Voltage Extraction. *IEEE Trans. Power Electron.* **2021**, *36*, 3757–3768. [CrossRef]
43. Zhang, L.; Liu, P.; Guo, S.; Huang, A.Q. Comparative Study of Temperature Sensitive Electrical Parameters (TSEP) of Si, SiC and GaN Power Devices. In Proceedings of the 2016 IEEE 4th Workshop on Wide Bandgap Power Devices and Applications (WiPDA), Fayetteville, AR, USA, 7–9 November 2016; pp. 302–307.